



**HAL**  
open science

## Interface evolution and performance degradation in LiCoO<sub>2</sub> composite battery electrodes monitored by advanced EQCM

Wanli Gao, Christel Laberty-Robert, Natacha Krins, Catherine Debiemme-Chouvy, Hubert Perrot, Ozlem Sel

► **To cite this version:**

Wanli Gao, Christel Laberty-Robert, Natacha Krins, Catherine Debiemme-Chouvy, Hubert Perrot, et al.. Interface evolution and performance degradation in LiCoO<sub>2</sub> composite battery electrodes monitored by advanced EQCM. *Electrochimica Acta*, 2022, 413, pp.140171. 10.1016/j.electacta.2022.140171 . hal-03602313

**HAL Id: hal-03602313**

**<https://hal.science/hal-03602313>**

Submitted on 10 Mar 2022

**HAL** is a multi-disciplinary open access archive for the deposit and dissemination of scientific research documents, whether they are published or not. The documents may come from teaching and research institutions in France or abroad, or from public or private research centers.

L'archive ouverte pluridisciplinaire **HAL**, est destinée au dépôt et à la diffusion de documents scientifiques de niveau recherche, publiés ou non, émanant des établissements d'enseignement et de recherche français ou étrangers, des laboratoires publics ou privés.

**Interface evolution and performance degradation in LiCoO<sub>2</sub> composite battery electrodes  
monitored by advanced EQCM**

Wanli Gao<sup>a</sup>, Christel Laberty-Robert<sup>b</sup>, Natacha Krins<sup>b</sup>, Catherine Debiemme-Chouvy<sup>a</sup>, Hubert Perrot<sup>a</sup> and Ozlem Sel<sup>a,c,\*</sup> sel.ozlem@gmail.com, ozlem.sel@sorbonne-universite.fr

<sup>a</sup>Sorbonne Université, CNRS, Laboratoire Interfaces et Systèmes Electrochimiques, 75005 Paris, France

<sup>b</sup>Sorbonne Université, CNRS, Laboratoire de Chimie de la Matière Condensée de Paris, 75005 Paris, France

<sup>c</sup>Chimie du Solide et de l'Energie, UMR 8260, Collège de France, 11 Place Marcelin Berthelot, 75231 cedex 05 Paris, France

\*Corresponding Author

**Abstract**

Unravelling the underlying reasons for degradation mechanism of battery materials is of great fundamental and practical importance. For a classical electrode consisting of an active material, a conductive additive, and a polymeric binder, its capacity fading is commonly related with (i) mechanical degradation of polymeric binder and/or (ii) structural and compositional degradation of active materials. The former is more relevant for electrodes showing volume expansion and represented by the progressive breakage of polymeric binder network during battery operation, leading to the dissolution of the other two components into electrolytes. The latter is generally reflected by an irreversible phase transition in active materials, which may affect the species exchanged at the electrode/electrolyte interface and their interfacial transfer dynamics. By

employing a coupled methodology pairing electrochemical techniques with piezoelectric probes derived from quartz crystal microbalance (QCM), this work reports on the evolution of the interfacial processes during electrochemical cycling and correlates to the performance degradation of the electrodes. Shown on a  $\text{LiCoO}_2$  (LCO) composite electrode as a model system, it was revealed that bare  $\text{Li}^+$  without a hydration sheath plays a dominant role in charge balance irrespective of the aging degree of the electrode under the experimental conditions of this work. However,  $\text{Li}^+$  transfer is closely accompanied with free  $\text{H}_2\text{O}$  molecules with a  $\text{Li}^+:\text{H}_2\text{O}$  ratio around 10:1 at a polarization state close to LCO redox potential (0.65 V vs. Ag/AgCl). This ratio persists in all cycled electrodes with gradually faded interfacial transfer kinetics of  $\text{Li}^+$  and  $\text{H}_2\text{O}$  along cycling. Such a fading in species interfacial transfer kinetics driven by the surficial evolution from  $\text{LiCoO}_2$  to  $\text{CoO}$  plays a major role in the electrode performance degradation during cycling.

## Keywords

Aqueous Li-ion batteries, Lithium cobalt oxide, degradation mechanism, interfacial ion transfer, EQCM

## 1. Introduction

Aqueous Li-ion batteries (Aqu-LIBs) continue to garner attention for grid-scale stationary energy storage system (EES) due to the multiple merits of environmentally benign water-based electrolytes, which outperforms their organic counterparts in terms of safety, cost efficiency, and ecofriendliness [1-4]. Significant progress has been made to optimize electrochemical performance of Aqu-LIBs constructed with commonly used cathode materials, such as  $\text{LiCoO}_2$  [5],  $\text{LiFePO}_4$  [6], and  $\text{LiMn}_2\text{O}_4$  [7]. This is exemplified by the introduction of highly concentrated electrolytes [7], electrode surface engineering by coating with protective layers [8], and structural design using three-dimensional electrodes [9], which, altogether, enables the feasibility of Aqu-LIBs with expanded voltage

window, improved long-term cyclability, and fast charge transfer for practical applications. In spite of recent improvements, a thorough understanding of the aqueous battery chemistry still remains elusive, the electrode degradation is commonly related with the electrode's mechanical fading and irreversible structural modifications of active materials during cycling. However, the interplay between the ion-solvent co-intercalation process and the electrode degradation is not entirely clear.

With the aim of shedding light on the operation and failure mechanisms, considerable efforts have been devoted with a number of *ex situ* and *in situ/operando* analytical tools. Using these *ex situ* characterization techniques (such as X-ray photoelectron spectroscopy (XPS) [10], atomic force microscopy (AFM) [11], and transmission X-ray microscopy (TXM) [12]) restricts the realistic information to be provided during an electrochemical process due to their intrinsic limitations, such as disconnection from the circuit and resultant relaxation phenomena. When employed during battery operation, *in situ* nuclear magnetic resonance (NMR) [13], *in situ* synchrotron and neutron techniques [14], *in situ* vibrational spectroscopy (such as *in situ* FTIR and *in situ* Raman) [15], *in situ* X-ray absorption spectroscopy (XAS) [16], and *in situ* scanning electron microscopy (SEM) [17] provide valuable real-time information regarding the structural, compositional and morphological evolution of the battery components.

The other crucial information to be monitored during cycling is the evolution of interfacial processes, such as the nature of the species transferred (solvated ions and/or bare ions), their interfacial transfer kinetics or resistance, the number of available electrochemically active sites. Additionally, of great fundamental importance but scarcely touched are the mechanical properties of electrode upon cycling. Periodical ion insertion/extraction results in dimensional changes in cycled electrodes, which are generally not entirely relaxed at the end of each cycle and tend to

gradually accumulate in the bulk of electrodes [6, 18]. This leads to the loss of capacity due to the progressive breakage of polymeric binder network, which concomitantly causes the contact loss between active materials and conductive carbon additives, and even their dissolution into electrolytes accompanied with modification of electrode/electrolyte interface (EEI). Within this context, experimental techniques providing (i) *in situ* quantitative analyses on interfacial behavior of species transfer and (ii) mechanical evolutions upon electrode cycling are highly desired.

Among the baseline characterization tools, electrochemical quartz crystal microbalance (EQCM) [19-24] and its non-classical coupling with electrochemical impedance spectroscopy (EIS), the so-called *ac*-electrogravimetry have been proposed as an effective probe for *in situ* capturing of species interfacial transfer behavior in various electrodes since its emergence in 1986 [25]. By virtue of coupling QCM with EIS and benefiting from this frequency-dependent measurement, *ac*-electrogravimetry provides several additional information such as (i) the species transferred at the interfaces to be identified by their molar mass and (ii) the interfacial kinetics of these species estimated thanks to this time-resolved method. In addition to the coupled methods based on gravimetric EQCM, multiharmonic EQCM with dissipation monitoring (EQCM-D) [26-30], has demonstrated itself as an effective probe for gravimetric, morphological and mechanical analyses for battery electrodes. Alike EQCM-D, the electroacoustic impedance is another QCM-derived method which enables its use as a morphological and mechanical probe [31, 32]. Two viscoelastic parameters of the electrode, *i.e.*, the storage ( $G'$ ) and loss modulus ( $G''$ ) can be estimated, corresponding to the rigidity and viscosity of the electrode, respectively. Therefore, towards elucidating the capacity fading of the battery electrodes during cycling, this work proposes an approach combining EQCM, *ac*-electrogravimetry and electroacoustic impedance to study the

LiCoO<sub>2</sub> composite electrode degradation in Li<sub>2</sub>SO<sub>4</sub> aqueous electrolyte as a model system for Aqu-LIB *via* two perspectives: (i) mechanical degradation related with failure of polymeric binder network. It should be mentioned that, although the binder degradation is not the main source for LiCoO<sub>2</sub> electrode fading [33], its mechanical integrity should be carefully scrutinized in flooded EQCM cells to rule out the possible changes in the composite electrode stiffness as a function of the cycle number for the reliability of gravimetric EQCM. and (ii) structural degradation of active materials affecting the processes occurring at the electrode/electrolyte interface (*i.e.*, nature of the species exchanged and their interfacial transfer dynamics). The evolution of the interfacial processes monitored by electrogravimetric methods is investigated not only in relation to the electromechanical properties as a function of degree of aging of the electrodes, but also to the results of compositional and structural property analyses performed on fresh and post-mortem electrodes. The proposed combined methodology provides a deep insight into the interplay between interfacial processes and LCO electrode degradation, studied as a model system, which then can be used as a powerful analytical platform for other battery chemistries.

## 2. Experimental Section

### 2.1. Preparation of LCO composite electrodes

The LCO composite electrodes were prepared according to our previously reported procedure [34]. Briefly, LCO (synthesized according to a hydrothermal protocol [35], where CoOOH synthesized in a former step was added into 0.5 mol/L LiOH in an autoclave and kept at 170 °C for 12 h), carbon black (Sigma-Aldrich) and poly(vinylidene fluoride)-co-hexafluoropropylene (PVDF-HFP) (Solef<sup>®</sup> 21508, Solvay Solexis, Italy) with a weight ratio of 8:1:1 was mixed with N-methylpyrrolidone (NMP) (Sigma-Aldrich) solvent in an agate mortar. The resultant suspension was drop-casted on the

gold electrode ( $0.2 \text{ cm}^2$ ) of the quartz resonator (9 MHz-AWS, Valencia, Spain) and dried at  $80 \text{ }^\circ\text{C}$  in an oven overnight. The mass loading was estimated by converting the microbalance frequency change ( $\Delta f$ ) to mass change ( $\Delta m$ ) before and after casting process in air by Sauerbrey equation [36], *i.e.*,  $\Delta f = -C_f \times \Delta m$ , where  $C_f$  is the experimental sensitivity factor of the quartz crystal resonator determined through copper electrodeposition ( $C_f = 16.3 \times 10^7 \text{ Hz.g}^{-1}.\text{cm}^2$ ) [37]. Typical loadings in this study were between  $12 \text{ }\mu\text{g}$  to  $14 \text{ }\mu\text{g}$ .

## 2.2 *In situ electrogravimetric measurements*

EQCM measurements were carried out with a three-electrode configuration using a lab-made QCM system coupled with a potentiostat (Biologic SP200). LCO composite electrode deposited as a thin layer on the quartz resonator (designated as LCO-loaded quartz) was used as the working electrode, platinum grid as the counter electrode and Ag/AgCl (3 M KCl saturated with AgCl) as the reference electrode. Unless otherwise specified, all potentials are *vs.* this reference electrode. Specifically, cyclic voltammetry (CV) coupled with QCM was performed in 1 M  $\text{Li}_2\text{SO}_4$  at a scan rate of  $0.5 \text{ mV}\cdot\text{s}^{-1}$ , with a potential window of 0.5 V and 0.9 V. The penetration depth of acoustic wave in the present EQCM measurements is 189 nm (calculated by  $\delta_n = (\eta_L / \pi n f_0 \rho_L)^{1/2}$ ,  $\eta_L$  and  $\rho_L$  are the dynamic viscosity and density of electrolyte,  $n$  is overtone order, which is 1 in our case,  $f_0$  is the fundamental frequency) [27].

As displayed in **Scheme 1**, four CV cycles were run to get a stable and reproducible electrochemical signature prior to and after cycling performance test (4<sup>th</sup> cycle was used for analysis). The CV response of a bare Au patterned quartz resonator is given in **Figure S1** in Supporting Information file. To evaluate the cycling performance, galvanostatic charge-discharge (GCD) coupled with QCM measurements were performed at a current density of  $0.075 \text{ mA cm}^{-2}$  (corresponding to  $\sim$

1.1 A g<sup>-1</sup> based on the mass of LCO composite electrode, and a discharge rate of ~14 C; a rate of nC corresponds to a full discharge in 1/n h). The electrogravimetric reliability of LCO composite electrodes has been verified in our prior work by the ratio of the motional resistance change ( $\Delta R_m$ ) to microbalance frequency change ( $\Delta f$ ) for LCO-loaded quartz resonator (with respect to the bare resonators) in 1 M Li<sub>2</sub>SO<sub>4</sub> [34], which gives a value of  $\Delta R_m/\Delta f < 0.01 \Omega \text{ Hz}^{-1}$  (upper limit for 9 MHz resonators [38]). Additionally, the condition of the gravimetric sensing was also verified by converting the recorded motional resistance change to full width at half height of the resonance peak,  $\Delta W$  (where  $\Delta W/2 = \Delta \Gamma$ , the half-width at half height of the resonance peak) [39]. The calculated value for a bare and a loaded resonator in air and in 1M Li<sub>2</sub>SO<sub>4</sub> follows the condition of  $|\Delta W| \ll |\Delta f/n|$ . The details can be found in the Supplementary Information file (**Equation S1** and **Table S1**). For *ac*-electrogravimetric measurements [40-45], a four-channel frequency response analyzer (FRA, Solartron 1254) and a lab-made potentiostat (SOTELEM-PGSTAT) were used. The QCM was performed under dynamic regime, and the modified working electrode was polarized at a selected potential (0.65 V, close to the CV peak potentials of LCO composite electrode, justified in the Results and Discussion part) to which a sinusoidal small amplitude potential perturbation (80 mV) was superimposed. The frequency range was between 63 kHz and 10 MHz. The mass change,  $\Delta m$ , of the working electrode was measured simultaneously with the *ac* response,  $\Delta I$ , of the electrochemical system. The experimental electrogravimetric transfer function (TF),  $\Delta m/\Delta E(\omega)$ , and the electrochemical impedance,  $\Delta E/\Delta I(\omega)$ , were obtained simultaneously at a given potential and frequency modulation,  $f$  (pulsation,  $\omega=2\pi f$ ). The  $\Delta E/\Delta I(\omega)$  was presented as the charge/potential TF,  $\Delta q/\Delta E(\omega)$ , which is more convenient to decouple the contribution of the various charged species. In charge/potential TF, each loop corresponds to one charged species, provided that their kinetics of

transfer are adequately different. The  $\Delta m/\Delta E(\omega)$  can identify both charged and uncharged species and provide the parameters related to their interfacial transfer. Details of the methodology can be found in previous papers [40-45].

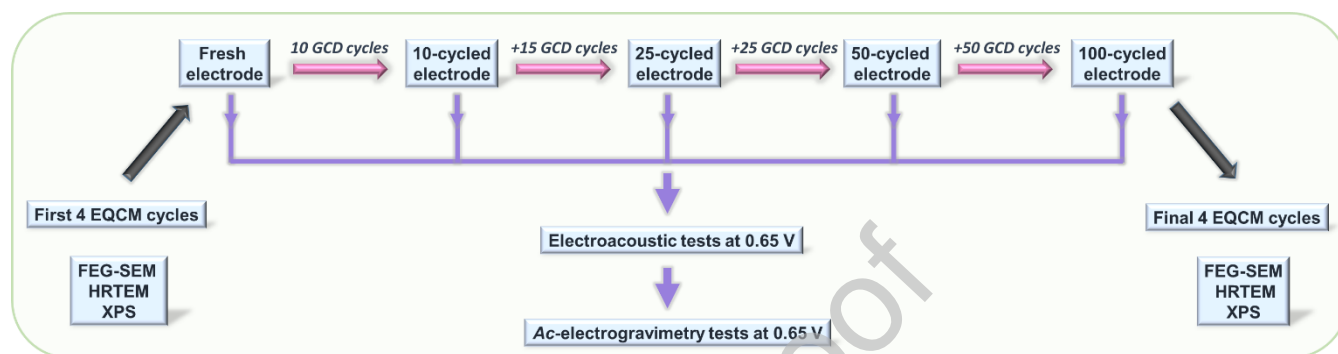
### 2.3. Probing mechanical properties by electroacoustic admittance analysis

The electroacoustic admittance measurements were conducted by an Agilent 4294A impedance analyzer coupled with a lab-made potentiostat (SOTELEM-PGSTAT) to track the electrode's viscoelastic changes at different degree of aging (fresh, 10-, 25-, 50-, and 100-time cycled states) (**Scheme 1**). A lab-made software (Simad) was used to fit the experimental electroacoustic admittance,  $Y_{exp}(\omega)$ , and theoretical one,  $Y_{th}(\omega)$ , of quartz resonator both in air and in solution. By this way, the storage modulus ( $G'$ ) and the loss modulus ( $G''$ ) of the LCO composite electrodes can be extracted. The Granstaff-Martin's model based on the transmission line modelling (TLM) is used here [46]. Specifically, four parameters of the LCO composite electrode are considered in the fitting process, *i.e.*, film thickness ( $d_f$ ), film density ( $\rho_f$ ),  $G'$  and  $G''$  of the LCO composite electrodes [47-50].

### 2.4. Morphological and structural characterizations

The morphological aspects of the LCO-coated quartz resonators were observed under vacuum conditions using a field emission gun scanning electron microscope (FEG-SEM, Zeiss, Supra 55). High resolution transmission electron microscopy (HRTEM) analysis was performed using a JEOL 2010 UHR microscope operating at 200 kV equipped with a TCD camera. X-ray photoelectron spectroscopy (XPS) analyses were performed using an Omicron Argus X-ray photoelectron spectrometer with monochromatized Al K $\alpha$  excitation (1486.6 eV) with a pass energy of 100 and 20 eV for acquisition of the survey and high-resolution spectra, respectively. In order to determine the

atomic surface composition, element peak intensities were corrected by Scofield factors [51] after baseline subtraction using the Shirley method. The spectra were fitted by using Casa XPS v.2.3.15 software. Above mentioned analyses were performed on the both fresh and 100-time cycled electrodes.



**Scheme 1.** Illustration of the measurement procedure to monitor the evolution of the LCO composite electrode which involves EQCM, galvanostatic charge-discharge (GCD), electroacoustic and *ac*-electrogravimetric tests during electrode cycling, as well as morphological and structural analyses on the fresh and cycled electrode.

### 3. Results and discussion

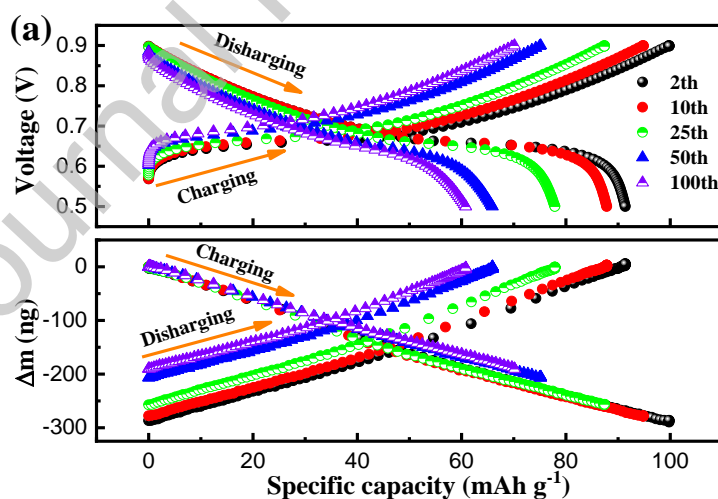
#### 3.1. *In situ* electrogravimetric study of LCO composite electrodes during cycling

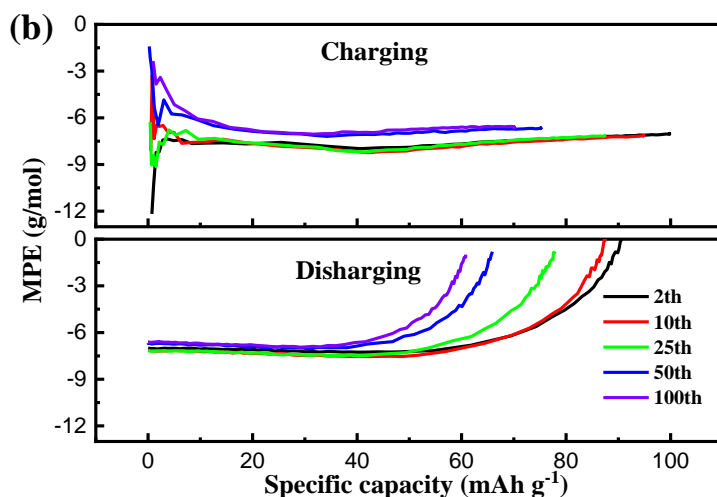
The cycling performance of LCO composite materials was studied by employing a gold-coated quartz resonator as a current collector to obtain (i) electrochemical signature simultaneously with (ii) resonant frequency changes ( $\Delta f$ ) corresponding to an electrochemical reaction at the EEI. A capacity fading of LCO composite electrodes with cycling was evidenced by the progressive shortening and growing separation of the charging/discharging profiles with cycling (upper panel in **Figure 1a**). Specifically, the charge/discharge behavior of 2-time cycled electrode shows one pair of plateau regions between 0.64 and 0.67 V, and delivers a specific capacity of  $91.4 \text{ mAh g}^{-1}$  at  $1.1 \text{ A g}^{-1}$ , which only remains 66.5% after 100 cycles. Such fast capacity degradation can be ascribed to a low

loading of LCO composite materials (to obtain a thin coating for EQCM studies) and to the flooded EQCM cell. The “floodness factor ( $S_{\text{flood}}$ )” is defined as the ratio of the mass of the solution to the mass of the immersed electrode [26], which is higher in the most EQCM research cells compared to the non-flooded coin cells. The influence of  $S_{\text{flood}}$  on the solid/electrolyte interphase (SEI) formation on  $\text{Li}_4\text{Ti}_5\text{O}_{12}$  electrodes were systematically studied by Dargel *et al.*, for different electrolyte compositions ( $\text{LiTFSI}$ ,  $\text{LiPF}_6$ , and  $\text{LiPF}_6$  +2% vinylene carbonate dissolved in EC +DMC (ethylene carbonate + dimethyl carbonate, 1:1 v/v)) [26]. The short time EQCM-D experiments revealed that the quality of SEI on LTO electrode was enhanced following the order of  $\text{LiPF}_6 < \text{LiPF}_6 + 2\%$  vinylene carbonate  $\ll \text{LiTFSI}$ . An analogous trend was confirmed by the coin-cell experiments, however, after many hundreds of cycles [26]. Thus, relatively high  $S_{\text{flood}}$  in this EQCM study can have an effect and accelerate the deterioration of reversible capacity of LCO composite electrodes in aqueous electrolytes (**Figure 1**).

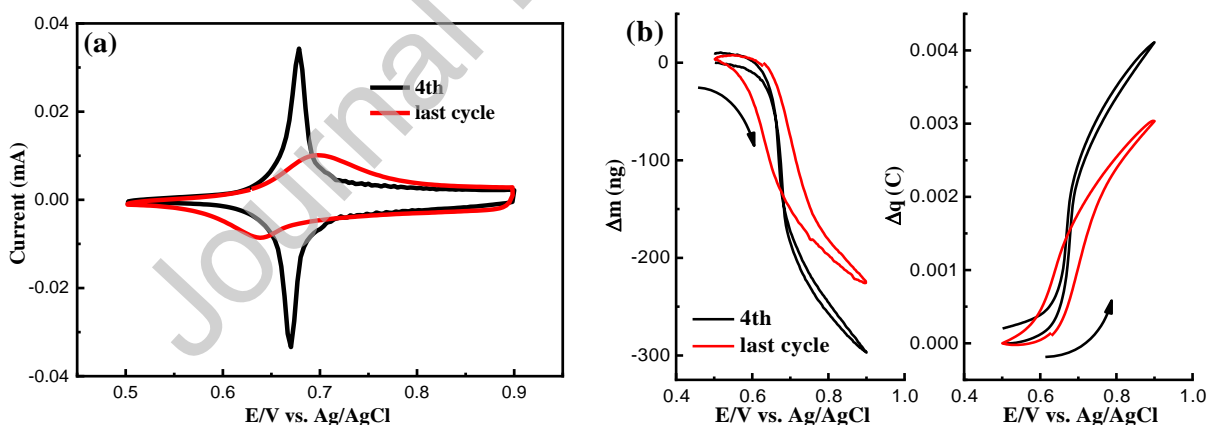
Additionally, benefited from the QCM coupling to electrochemical tests, the electrode mass changes were also simultaneously recorded during cycling (down panel in **Figure 1a**). The  $\text{Li}^+$  deintercalation out of and intercalation into the electrode ( $\text{LiCoO}_2 \leftrightarrow \text{Li}_{1-x}\text{CoO}_2 + x\text{Li}^+ + xe^-$ ) is reflected by a mass egress/ingress during charging/discharging process. Besides, consistent with the capacity fading, a concomitant fading in exchanged mass is also observed during cycling. For example, a total of  $\sim 290$  ng can be exchanged during charging/discharging process for 2-time cycled electrode, which only remains 191 ng after 100 cycles (34.5% loss). To further explore the nature of the exchanged species during an electrochemical process, the average mass per mole of electrons ( $MPE = F \times (\Delta m/\Delta q)$ ) was estimated from EQCM data. Theoretically, only one ionic participant in charge compensation leads to the absolute MPE value as equivalent to its molar mass,

with negative and positive signs for cations and anions, respectively. **Figure 1b** shows electrodes with different degree of cycling present close MPE values with slight deviation between  $-8 \text{ g}\cdot\text{mol}^{-1}$  to  $-6.5 \text{ g}\cdot\text{mol}^{-1}$ , indicating that the  $\text{Li}^+$  (with an MPE of  $\sim -7 \text{ g}\cdot\text{mol}^{-1}$ ) is the dominating species at the EEI irrespective of the electrode degradation level. It is worth mentioning that, only around the charge/discharge plateau potential, the MPE close to  $-7$  remains roughly constant. This is because the majority of  $\text{Li}^+$  ions are exchanged during this potential range. However, the amount of the exchanged  $\text{Li}^+$  ions is significantly decreased out of the charge/discharge plateau potential. In this case, the MPE can be sensitively affected by other species transfer. This is especially obvious when the amount of exchanged  $\text{Li}^+$  is low, which corresponds to the non-plateau capacity region. This non-plateau region is mainly related to the beginning of charge and the end of discharge. The possibility of the presence of other species, *i.e.*, multispecies contribution to the charge compensation process will be evaluated by using *ac*-electrogravimetric analyses.





**Figure 1.** Galvanostatic charge-discharge curves coupled with QCM measurements leading to simultaneously obtained mass changes of LCO composite electrode at  $0.075 \text{ mA cm}^{-2}$  (corresponding to  $\sim 1.1 \text{ A g}^{-1}$  based on the mass of LCO composite materials). (a) Comparison of charge-discharge curves (upper panel) among 2nd, 10th, 25th, 50th and 100th cycle with corresponding mass changes (down panel). (b) Average mass per mole of electrons (*MPE*) calculated from EQCM data during charge-discharge process of electrodes at different cycled states.



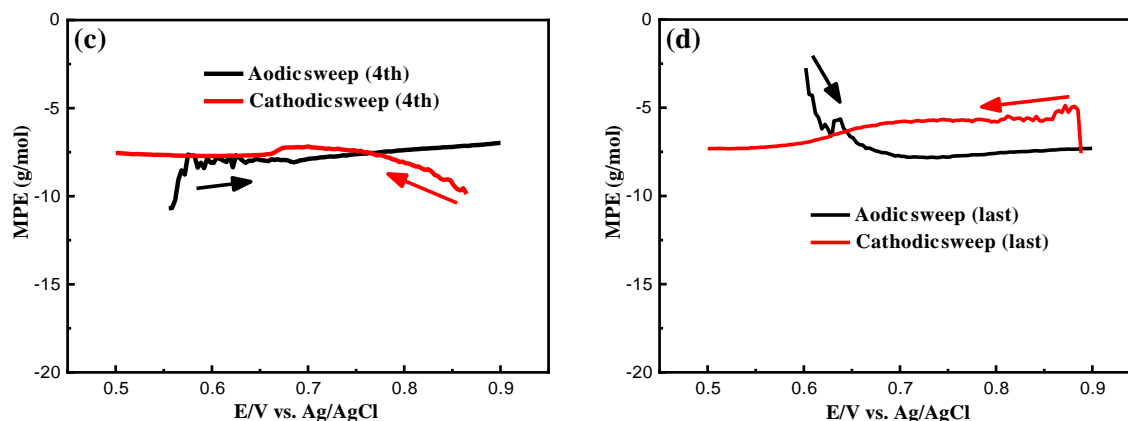


**Figure 2.** Comparison of CV curves (a) and simultaneously obtained mass responses (b, left panel) and corresponding charge change (b, right panel) of fresh and aged electrode (100-time cycled electrode) in 1 M  $\text{Li}_2\text{SO}_4$  solution at  $0.5 \text{ mV s}^{-1}$ . Panel (c) and (d) are the corresponding MPE values of fresh and aged electrode, respectively, calculated from EOCM data.

**Figure 2** compares the cyclic voltammetry (CV) profiles of LCO composite electrode prior to and after charging-discharging measurements (fresh and 100-time cycled electrode). The CV profile of fresh electrode shows one correlative couple of redox peaks between 0.65 and 0.70 V (**Figure 2a**) that are identified in the charging-discharging curves, corresponding to the deintercalation/intercalation process of  $\text{Li}^+$  ions. Such small peak separation of fresh LCO composite electrode indicates a sufficient kinetics of electron transfer in fresh LCO composite electrode on Au-coated quartz resonators and high  $\text{Li}^+$  transfer kinetics at electrode/electrolyte interface. After 100 charge-discharge cycles, a drastic decrease in current intensity with the enlarged peak separation is observed, indicating deteriorated electrode kinetics during cycling [52]. This resultantly leads to a smaller charge variation during one CV cycle from 4.1 mC to 3.1 mC (**Figure 2b**, left panel), and a decrease in  $\Delta m$  from 297 ng for the fresh electrode to 226 ng for the 100-time cycled electrode (**Figure 2b**, right panel), together with weakened reversible electrogravimetric behavior between cathodic and anodic scan (different from the roughly overlapped  $\Delta m$ -E curves for

fresh electrode). Besides, both fresh and 100-time cycled electrodes present a comparable MPE of  $\sim -7.5 \text{ g}\cdot\text{mol}^{-1}$  as identified in GCD tests, further indicating that the nature of exchanged species in charge compensation process is likely to remain the same. Then, other possible reasons behind the capacity decay observed in **Figure 1** and **Figure 2** are scrutinized in the following.

### **3.2. Investigation of the origin of the capacity decay in LCO composite electrode**

The composite electrode degradation is commonly related with (i) mechanical fading, represented by the breakage of polymeric binder network, loss of the contact between the particles (active material/ conductive carbon) and resultant dissolution of active materials (macroscopic changes), (ii) structural fading of active materials or (iii) changes of the electrode/electrolyte interface processes (microscopic changes). Briefly, to assess the fault to capacity fading, three different hypotheses related to (a) mechanical properties, (b) structural/morphological evolution and (c) interfacial processes are scrutinized. The evolution of mechanical properties, structural/morphological characteristics and interfacial processes as a function of cycling are monitored by the corresponding investigation techniques: electroacoustic impedance, SEM-FEG, HR-TEM, XPS, EQCM and *ac*-electrogravimetry measurements, as described in **Scheme 1**.

#### **3.2.1 Monitoring macroscopic mechanical properties during electrochemical cycling by electroacoustic impedance**

To address the possible correlation between electrode capacity fading and its macroscopic mechanical changes, the electrode's viscoelastic changes during cycling was firstly studied by tracking the evolution of two viscoelastic parameters, storage modulus ( $G'$ ) and loss modulus ( $G''$ ) (**Figure 3**) [31, 53-55]. A fitting example for fresh LCO composite electrode polarized at 0.65 V is presented in **Figure 3a**. It shows a good agreement between the real and imaginary part of

experimental and fitted electroacoustic admittance,  $G$  and  $B$ , over the frequency. Following the same fitting procedure, the mechanical evolution of the composite electrode is estimated (**Figure 3b**).  $G'$  is ca. two times larger than  $G''$  and both remain roughly constant during cycling, with slight deviation from  $2.07$  to  $1.97 \times 10^6 \text{ N.m}^{-2}$ , and from  $1.26$  to  $1.10 \times 10^6 \text{ N.m}^{-2}$ , respectively. This evolution is comparable to what has been observed in  $\text{LiFePO}_4$  composite electrodes [53]. It implies the rigidity and viscosity of LCO composite electrode remains almost constant during the experiments performed in this study (100 cycles), which is in line with the results obtained for another composite electrode, made of  $\text{LiFePO}_4$  with PVDF binder tested in aqueous  $\text{Li}_2\text{SO}_4$  electrolyte [54]. The progressive minor decrease of  $G'$  and  $G''$  (thus complex shear modulus as well) indicates a very slight electrode softening probably due to the impregnation of electrode by the electrolyte during cycling. Such slight softening is considered negligible and could not bring significant effect on the gravimetric interpretation using Sauerbrey equation. It can thus be concluded that LCO composite electrode remains rigid and capacity fading is not linked to the electrode mechanical degradation in the current study. This result is in line with the fact that the binder effect is much significant when large volume changes take place (*i.e.*, Si electrodes or insertion of  $\text{Na}^+$  into  $\text{FePO}_4$ ).

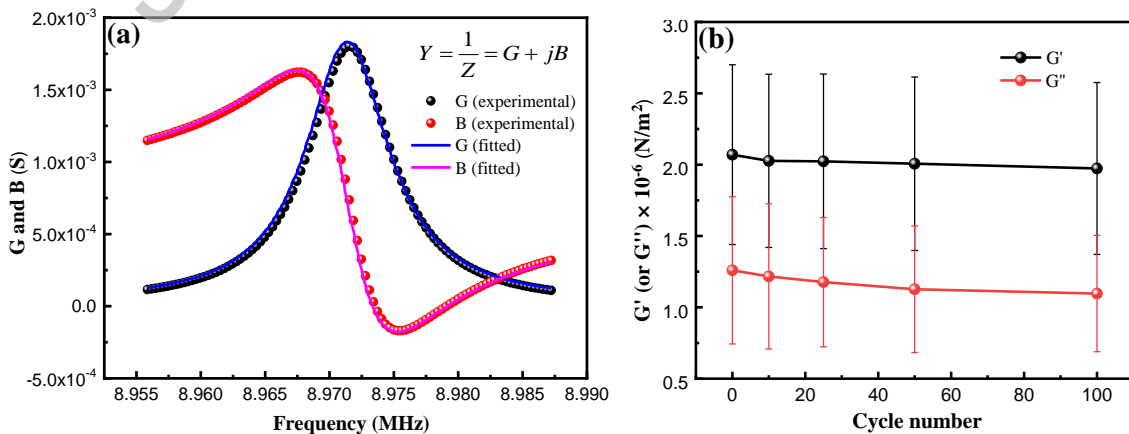


**Figure 3.** (a) Electroacoustic admittance measurements: experimental and fitted conductance and

susceptance,  $G$  and  $B$ , over frequency for fresh  $\text{LiCoO}_2$  composite electrode at 0.65 V. Fitting parameters:  $G' = 2.34 \times 10^6 \text{ N.m}^{-2}$ ,  $G'' = 1.85 \times 10^6 \text{ N.m}^{-2}$ ,  $d_f = 300 \text{ nm}$  and  $\rho_f = 3.1 \text{ g.cm}^{-3}$  ( $\rho_f$  is kept constant during fitting process). (b) Evolution of real ( $G'$ ) and imaginary ( $G''$ ) components of complex shear modulus of LCO composite electrode during cycling. The error bar was obtained from 3 electrodes with loading of 11.2, 13.8 and 14.0  $\mu\text{g}$ , respectively.

### 3.2.2 Evolution of structural and compositional characteristics

The morphology of LCO composite electrode before and after electrochemical tests were firstly compared by FEG-SEM (**Figure 4**). A good coverage of LCO composite materials on gold-coated quartz resonator was observed for as-prepared electrode, which remained in 100-time cycled electrode. Besides, higher-magnification images (**Figure 4c** and **d**) show no obvious morphology change before and after cycling tests. This implies no significant dissolution of LCO composite materials into the electrolyte occurs, indirectly confirming the well-remained polymeric binder network during electrochemical tests in current study. This point was also verified by the roughly constant frequency (with only 200 Hz variation) at different cycled electrode during electroacoustic measurements. To get insight into how the structure and interfacial composition is affected by cycling,

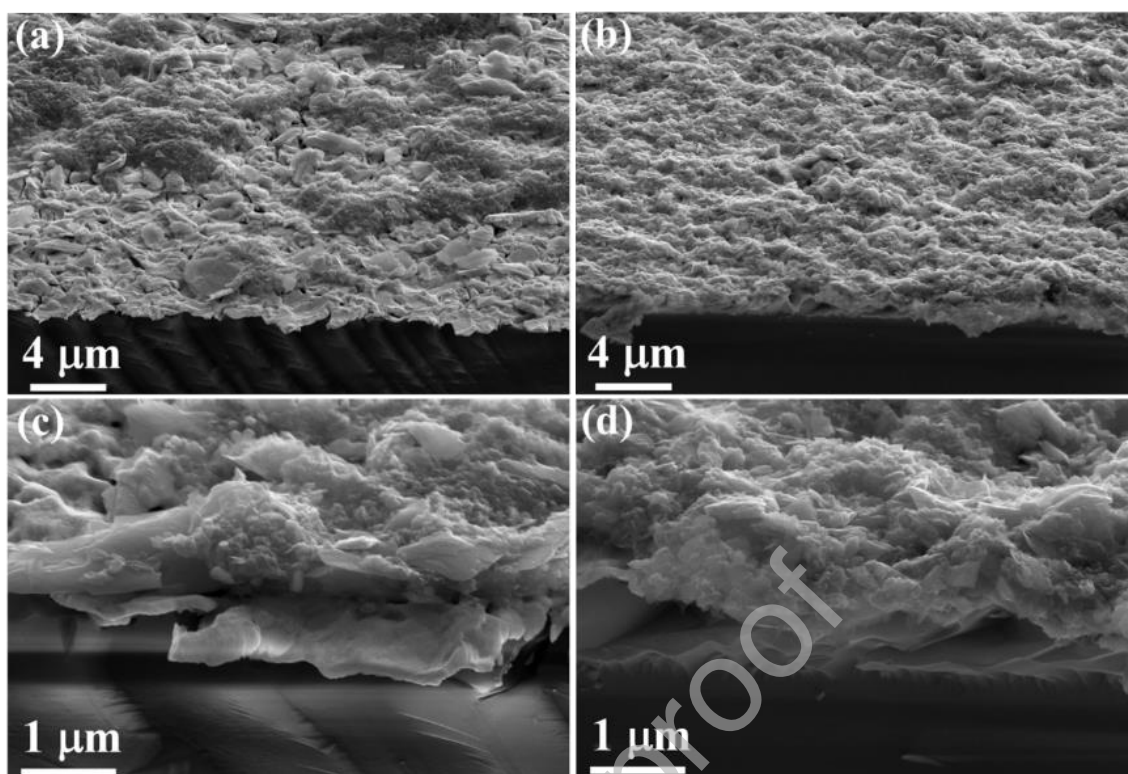


**Figure 4.** FEG-SEM micrographs and morphological observations of as-prepared (a, c) and 100-time cycled (b, d) LCO composite electrode.

post-mortem analyses by HR-TEM and XPS (**Figure 5**) were further performed. Crystal planes with a *d-spacing* of 0.47 nm were observed to extend up to the surface of as-prepared LCO composite electrode (**Figure 5a**). However, a noticeable phase change was identified on the surface of 100-time cycled electrode (**Figure 5b**), which was reflected by a significant transition in crystal plane spacing from 0.47 nm to 0.24 nm, corresponding to a phase transition from (003) planes in bulk LCO to (111) planes in surface CoO [5]. To further elucidate the formation of CoO on the surface of LCO during cycling, a surface-sensitive technique, XPS, was used. O1s spectrum of as-prepared electrode displays three components, O-Co (~529.4 eV) from the LCO crystalline network [56], the oxygen functional group C=O and LCO surface O (~531.5 eV), and another oxygen functional group C-O (~532.8 eV) (**Figure 5c and d**). The fraction of the O1s peak corresponding to O–Co bond can be evaluated as the fraction of O-Co area under the O1s curve [5].

This fraction is multiplied with the atomic percentage obtained from the O1s high resolution spectrum to obtain the actual contribution of oxygen to the O–Co bond. The Co atomic percentage is directly obtained from the Co2p high

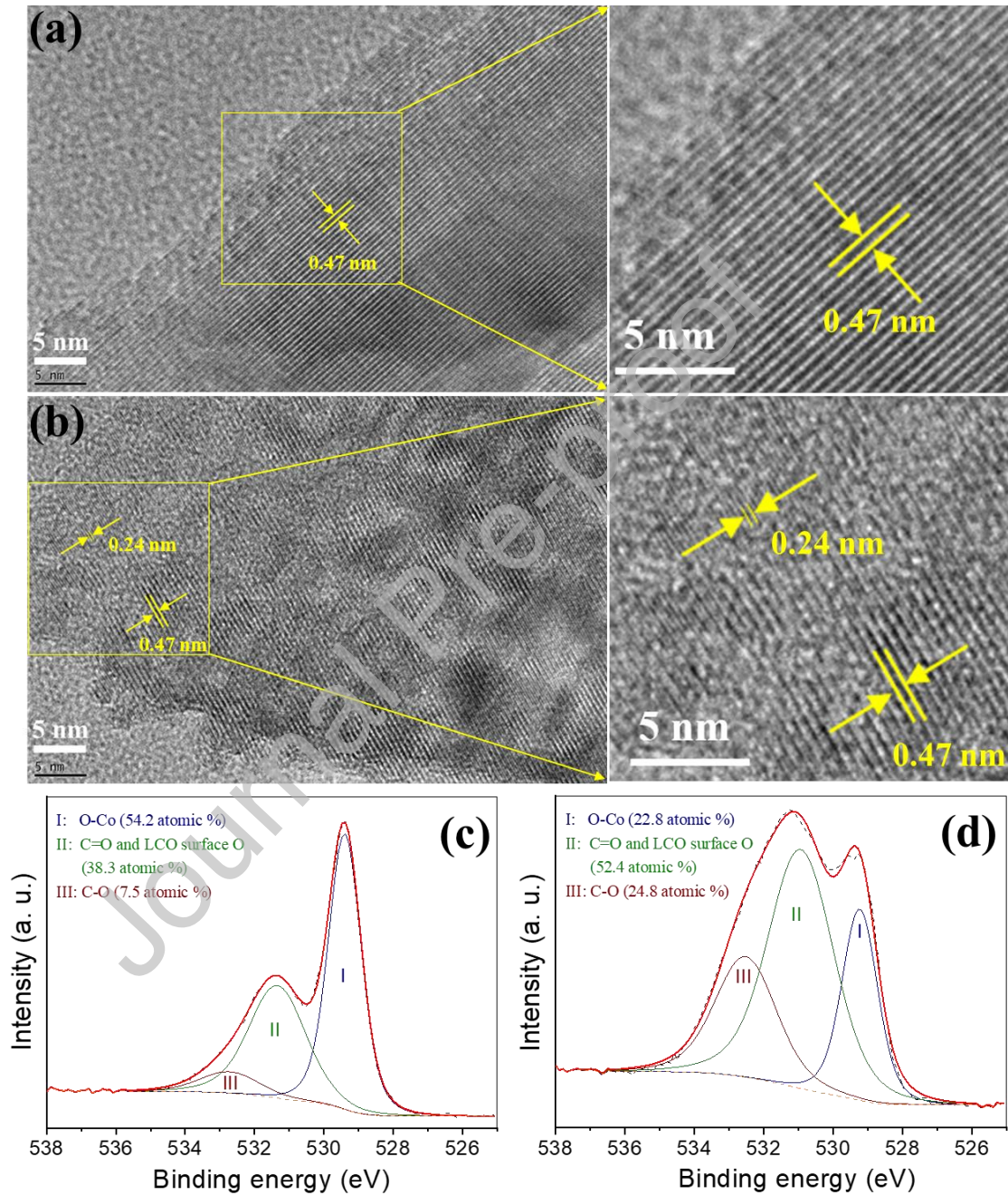


**Figure 5.** (a) and (b) HRTEM images of as-prepared and final cycled LCO particle. XPS spectra for O1s peaks in (c) fresh and (d) 100-time cycled LCO electrodes.

resolution spectrum and summarized in **Table S2**. Then, the ratio of O:Co can be calculated. As anticipated, the as-presented LCO composite electrode gives the O:Co value of  $\sim 1.57$ , close to the theoretical value of 2 based on the stoichiometric LCO ( $\text{LiCoO}_2$ ). After 100 cycles, this ratio decreases to  $\sim 1.19$ , approaching the theoretical value of 1 according to the stoichiometric CoO. This indicates a gradual surficial modification from  $\text{Co}^{(3+)}$  to  $\text{Co}^{(2+)}$  occurring during electrode cycling by converting LCO to CoO, which is in agreement with previous work on the degradation mechanism of LCO electrode in aqueous electrolytes.[5] However, how exactly this surficial evolution from LCO to CoO affects the  $\text{Li}^+$  interfacial transfer behavior has never fundamentally studied, which is primarily due to the limitation of well-suitable analytical tools. Therefore, a deeper understanding of  $\text{Li}^+$  transfer behavior at EEI during electrode degradation process is highly desired. Additionally, the  $\text{H}_2\text{O}$  molecules are commonly reported to accompany cations transfer by “co-intercalation”, [57] [58] [59] but how  $\text{H}_2\text{O}$  molecules participate in charge balance process (*via* hydration sheath or in free form) during electrode degradation process remains another challenge. To answer the aforementioned questions, *ac*-electrogravimetry demonstrates its advantages benefiting from the frequency-dependent electrogravimetric measurement, which enables the deconvolution of the species contributions with their transfer kinetics.

### **3.2.3 Monitoring the evolution of interfacial properties during electrochemical cycling by *ac*-electrogravimetry**

The effect of surficial LCO to CoO evolution on the  $\text{Li}^+$  interfacial transfer behavior is investigated by *ac*-electrogravimetry. By coupling QCM with EIS, *ac*-electrogravimetry, makes it possible to disentangle the subtleties of interfacial transfer behavior of multi-species directly or indirectly involved in the charge compensation process. During an electrochemical process, the charged

species transfer is tracked by EIS, whereas both charged and non-charged species (such as free H<sub>2</sub>O molecules) transfer can be gravimetrically identified by QCM [40, 41]. Correspondingly, two important transfer functions (TFs), charge/potential TF ( $\Delta q/\Delta E(\omega)$ ) and mass/potential TF ( $\Delta m/\Delta E(\omega)$ ) are obtained. Derived from typical impedance ( $\Delta E/\Delta I(\omega)$ ),  $\Delta q/\Delta E(\omega)$  TF only considers the interfacial ionic species transfer in response to the potential perturbation, while the  $\Delta m/\Delta E(\omega)$  TF corresponds to the mass response of the electrode including non-charged free solvent contribution (**Figure 6**). Alike EIS analysis, a suitable configuration is needed to fit the *ac*-electrogravimetric experimental data to get parameters related with species interfacial transfer behavior. To fit the experimental data ( $\Delta q/\Delta E(\omega)$  and  $\Delta m/\Delta E(\omega)$ ) with theoretical expressions (**Equation S3** and **S4**), a configuration involving the transfer of cations (Li<sup>+</sup>), H<sub>2</sub>O molecules, and anions (SO<sub>4</sub><sup>2-</sup>) is proposed to achieve a good agreement between experimental and theoretical profiles both in terms of shape and frequencies. It should be highlighted that the species determination is revealed according to their molar mass ( $M_i$ ), which is involved in the electrogravimetric TF ( $\Delta m/\Delta E(\omega)$ , **Equation S4**). Three species (Li<sup>+</sup>, H<sub>2</sub>O, and SO<sub>4</sub><sup>2-</sup>) were identified in fresh electrode (**Figure 6b**). This is in line with our prior work, in which the species interfacial transfer behavior in fresh LCO composite electrode is studied [34].

With cycling, the transfer of these three species persists in electrodes with the different degree of aging, as exemplified in 25- and 100-time cycled electrode (**Figure 6d** and **f**, respectively). Only a progressive decrease in their quantities is observed, as reflected by the faded response in  $\Delta q/\Delta E(\omega)$  and  $\Delta m/\Delta E(\omega)$ . Furthermore, benefited from this frequency-dependent measurement, the kinetics information of species transfer is further investigated. In all electrodes with different aged states,

$\text{Li}^+$  cations are exchanged in higher frequency region than  $\text{H}_2\text{O}$  molecules and both present the same flux

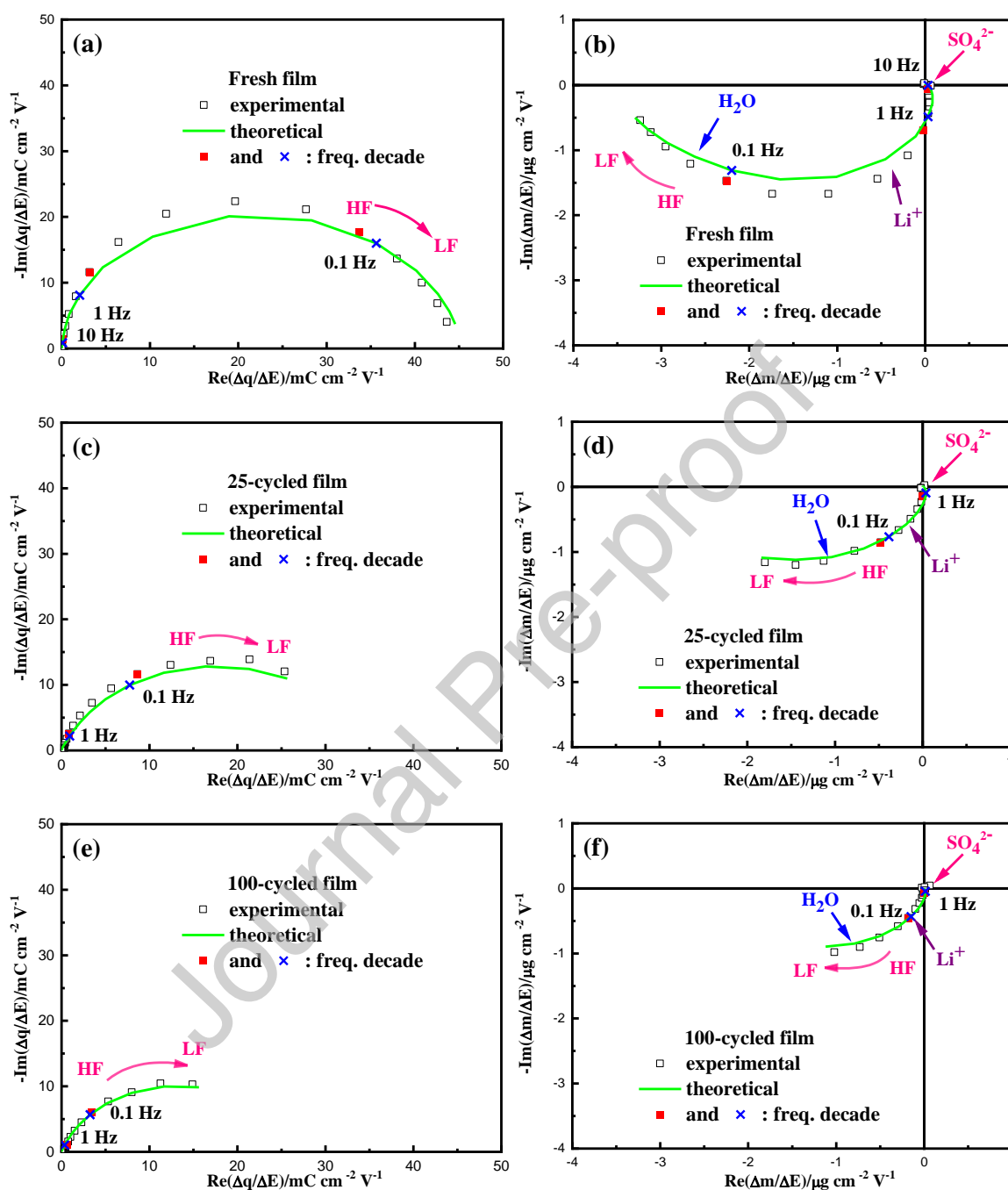


**Figure 6.** Theoretical and experimental (a, c, e)  $\Delta q/\Delta E(w)$  and (b, d, f)  $\Delta m/\Delta E(w)$  transfer functions at 0.65 V vs. Ag/AgCl of the LCO composite electrode at different aged states (HF: high frequency; LF: low frequency).  $\Delta q/\Delta E(w)$  shows the contribution from the charged species without any identification, whereas  $\Delta m/\Delta E(w)$  identifies charged and uncharged species with their atomic mass,

as well as their kinetics of transfer.

direction. It is worth mentioning that, instead of hydrated  $\text{Li}^+$  ( $\text{Li}^+ \cdot n\text{H}_2\text{O}$ ), in which  $\text{Li}^+$  cations and free  $\text{H}_2\text{O}$  molecules are exchanged in the exact same behavior (same concentration and kinetics),  $\text{Li}^+$  cations and free  $\text{H}_2\text{O}$  molecules are exchanged independently but with close transfer kinetics, since only one suppressed loop in  $\Delta m/\Delta E(\omega)$  TF is observed in **Figure 6b, d and f**. The close interaction leads to the hypothesis that the  $\text{H}_2\text{O}$  molecules assist the  $\text{Li}^+$  ions transfer at the LCO/electrolyte interface. This finding is supported by a synchronous evolution in absolute relative concentration changes peaking around redox potentials, as reported in our previous work [34]. Additionally, a very small amount of  $\text{SO}_4^{2-}$  anions was detected at high frequencies (HFs) in **Figure 6b, d and f**, signifying a fast interfacial transfer kinetics with an opposite flux direction to  $\text{Li}^+$  and  $\text{H}_2\text{O}$  transfer. The fast  $\text{SO}_4^{2-}$  transfer behavior is likely related to their fast surface-controlled electroadsorption process. The possible active sites for  $\text{SO}_4^{2-}$  transfer are micropores or microrough surface of the LCO composite electrode on the scale of penetration depth of acoustic wave (189 nm for these EQCM measurements), in which carbon black (composite electrode contains 10 wt%) and gold substrate surface (if accessible after coating with the LCO electrode) should be considered [34]. [34]. **Figure 7a** summarizes the transfer kinetics ( $K_i$ ) of electrodes at different aged states estimated at 0.65 V. In this work,  $\text{Li}^+$  exhibits a higher interfacial transfer kinetics than free  $\text{H}_2\text{O}$  molecules and both turn to decrease (particularly during first 25 cycles) in an almost parallel manner with electrode cycling. Besides, alike the evolution of  $K_i$ , a synchronously decreased concentration changes of each species ( $\Delta C_i$ ) with respect to the potential variation ( $\Delta E$ ), estimated through **Equation S2 and S5**, is found between  $\text{Li}^+$  cations and free  $\text{H}_2\text{O}$  molecules (**Figure 7b**). Importantly, the ratio of  $\text{Li}^+:\text{H}_2\text{O}$  remains roughly constant irrespective of the electrode's aging state, stabilizing

around 10:1 at the polarization state (0.65 V vs. Ag/AgCl) close to LCO redox peaks. This ratio persists in all cycled electrodes with only progressively faded interfacial transfer dynamics of  $\text{Li}^+$  and  $\text{H}_2\text{O}$  along cycling. This is supported by a similar  $\text{Li}^+:\text{H}_2\text{O}$  ratio of around 7:1 identified in fresh LCO composite electrode at the same polarized state in our previous work [34]. The difference of  $\text{Li}^+:\text{H}_2\text{O}$  ratio in this work is probably related with the different electrochemical history: instead of using potential window of 0.6-0.9 V in CV [34], this work extends to 0.5-0.9 V to visualize a more complete CV profile. This indicates a close interaction between  $\text{Li}^+$  cations and free  $\text{H}_2\text{O}$  molecules during interfacial transfer process remains irrespective of electrode aged states, and the faded  $K_i$  and decreased quantities of  $\text{Li}^+$  cations and free  $\text{H}_2\text{O}$  molecules required in charge balance are resulted from a gradual structural transition of active material (LCO) to passivation layer (CoO).

Overall, *ac*-electrogravimetry reveals that the global EQCM mass response is constituted of 3 different contributions, where the  $\text{Li}^+$  is the dominant species. The nature of the species ( $\text{SO}_4^{2-}$ ,  $\text{Li}^+$ , and free  $\text{H}_2\text{O}$ ) exchanged at the EEI remains the same independent of the number of cycling, but the species interfacial transfer becomes much slower, for instance, the transfer kinetics of  $\text{Li}^+$  is about 10 times lower after 100 cycles (**Figure 7a**). In **Figure 7b**, the  $|\Delta C_i/\Delta E|$  ratio values indicate that the anion ( $\text{SO}_4^{2-}$ ) contribution is minor, with a factor of  $\sim 100$  as compared to the cation ( $\text{Li}^+$ ), and the main contribution is related to this latter.

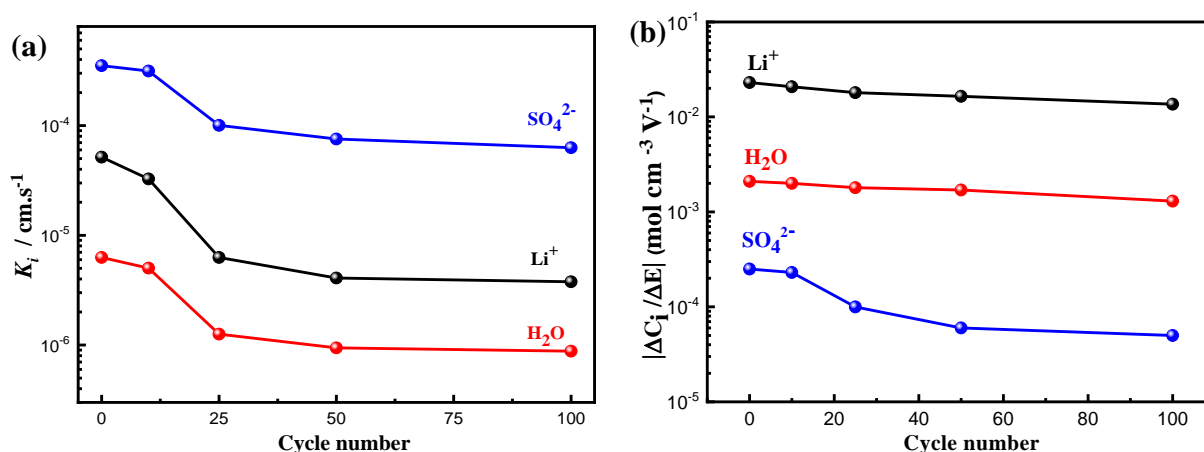


**Figure 7.** (a) Transfer kinetics,  $K_i$  ( $\text{cm}\cdot\text{s}^{-1}$ ) and (b)  $|\Delta C_i/\Delta E|$  ( $\text{mol cm}^{-3} \text{V}^{-1}$ ) as a function of cycle number for  $\text{SO}_4^{2-}$ ,  $\text{Li}^+$ , and  $\text{H}_2\text{O}$  participating in the electrochemical process.

#### 4. Conclusion

A thorough analysis expanding from the mechanical and interfacial properties to the structural/compositional changes was performed to unravel the reasons behind the capacity fading of composite electrodes in Aqu-LIBs. Shown on a classical LCO cathode material in  $\text{Li}_2\text{SO}_4$  as an example, QCM derived coupled methods (EQCM, *ac*-electrogravimetry, and electroacoustic impedance spectroscopy) were employed to study the influence of electrode cycling on its electrochemical, interfacial and mechanical property evolution. Our work revealed that instead of macroscopic mechanical degradation, the electrode capacity fading in present work is mainly ascribed to the structural degradation of LCO active material. Indeed, the structure at the nanoscale is altered and surface composition showed a certain evolution from LCO to CoO, as evidenced by HRTEM and XPS, respectively. Then, the effect of the surficial composition changes on the interfacial charge transfer properties (specifically the electrical double layer where the ions desolvation and then the transfer occur) was investigated. Our study shows that the structural evolution of the interface does not affect the nature of species exchanged at the electrode/electrolyte interface during charge balance, but significantly slows down their interfacial transfer dynamics (for

instance a kinetics-decreasing factor of  $\sim 10$  for  $\text{Li}^+$  at a fresh EEI compared to a 100-time cycled EEI) as attested by *ac*-electrogravimetry. This work provides a further understanding on the origin of the capacity decay, revealing that the compositional changes of the active material during electrode degradation slow down the EEI dynamics. The methodology can be employed to study other active material/electrolyte compositions and can be an effective approach for evaluating the strategies for alleviating the capacity loss such as surface coatings of active materials.

## ASSOCIATED CONTENT

Theoretical expressions used for fitting the *ac*-electrogravimetry data and additional XPS data of the LCO composite electrodes.

## AUTHOR INFORMATION

### Notes

The authors declare no competing financial interests.

### Credit CRediT author statement

**Wanli Gao:** Investigation, Formal analysis, Writing - Original Draft, Writing - Review & Editing;

**Christel Laberty-Robert:** Funding acquisition, Conceptualization, Formal analysis; **Natacha**

**Krins:** Formal analysis; **Catherine Debiemme-Chouvy:** Formal analysis; **Hubert Perrot:**

Development or design of methodology; creation of models, Resources; **Ozlem Sel:** Funding acquisition, Conceptualization, Supervision, Writing - Review & Editing

### Declaration of interests

The authors declare that they have no known competing financial interests or personal relationships that could have appeared to influence the work reported in this paper.

## ACKNOWLEDGMENT

This work was supported by the ANR under reference ANR-11-IDEX-0004-02 and by the Cluster of Excellence LABEX MATISSE led by Sorbonne Université. Françoise Pillier and Sandra Casale are acknowledged for FEG-SEM and HRTEM analyses, respectively.

## References

- [1] W. Li, J. R. Dahn, D.S. Wainwright, Rechargeable lithium batteries with aqueous electrolytes, *Science*, 264 (1994) 1115-1118.
- [2] C. Yang, J. Chen, X. Ji, T.P. Pollard, X. Lu, C.J. Sun, S. Hou, Q. Liu, C. Liu, T. Qing, Y. Wang, O. Borodin, Y. Ren, K. Xu, C. Wang, Aqueous Li-ion battery enabled by halogen conversion-intercalation chemistry in graphite, *Nature*, 569 (2019) 245-250.
- [3] R. Demir-Cakan, M.R. Palacin, L. Croguennec, Rechargeable aqueous electrolyte batteries: from univalent to multivalent cation chemistry, *J. Mater. Chem. A*, 7 (2019) 20519-20539.
- [4] D. Chao, W. Zhou, F. Xie, C. Ye, H. Li, M. Jaroniec, S.-Z. Qiao, Roadmap for Advanced Aqueous Batteries, *Sci. Adv.*, 6 (2020) eaba4098.
- [5] A. Ramanujapuram, D. Gordon, A. Magasinski, B. Ward, N. Nitta, C. Huang, G. Yushin, Degradation and stabilization of lithium cobalt oxide in aqueous electrolytes, *Energy Environ. Sci.*, 9 (2016) 1841-1848.
- [6] N. Shpigel, M.D. Levi, X. Cheng, T. Cao, R. Wu, T.S. Mathis, Y. Zhang, D. Aurbach, Y. Gogotsi, Diffusion-Induced Transient Stresses in Li-Battery Electrodes Imaged by Electrochemical Quartz Crystal Microbalance with Dissipation Monitoring and Environmental Scanning Electron Microscopy, *ACS Energy Lett.*, 4 (2019) 1907-1917.
- [7] L. Suo, O. Borodin, T. Gao, M. Olguin, J. Ho, X. Fan, C. Luo, C. Wang, K. Xu, "Water-in-salt" electrolyte enables high-voltage aqueous lithium-ion chemistries, *Science* 350 (2015) 938-943.
- [8] Q. Yang, J. Huang, Y. Li, Y. Wang, J. Qiu, J. Zhang, H. Yu, X. Yu, H. Li, L. Chen, Surface-protected LiCoO<sub>2</sub> with ultrathin solid oxide electrolyte film for high-voltage lithium ion batteries and lithium polymer batteries, *J. Power Sources*, 388 (2018) 65-70.
- [9] L. Xue, Q. Zhang, X. Zhu, L. Gu, J. Yue, Q. Xia, T. Xing, T. Chen, Y. Yao, H. Xia, 3D LiCoO<sub>2</sub> nanosheets assembled nanorod arrays via confined dissolution-recrystallization for advanced aqueous lithium-ion batteries, *Nano Energy*, 56 (2019) 463-472.
- [10] J.-N. Zhang, Q. Li, Y. Wang, J. Zheng, X. Yu, H. Li, Dynamic evolution of cathode electrolyte interphase (CEI) on high voltage LiCoO<sub>2</sub> cathode and its interaction with Li anode, *Energy Storage Mater.*, 14 (2018) 1-7.
- [11] H. Kang, J. Lee, T. Rodgers, J.-H. Shim, S. Lee, Electrical Conductivity of Delithiated Lithium Cobalt Oxides: Conductive Atomic Force Microscopy and Density Functional Theory Study, *J. Phys. Chem. C* 123 (2019) 17703-17710.
- [12] P.-C. Tsai, B. Wen, M. Wolfman, M.-J. Choe, M.S. Pan, L. Su, K. Thornton, J. Cabana, Y.-M. Chiang, Single-particle measurements of electrochemical kinetics in NMC and NCA cathodes for Li-ion batteries, *Energy Environ. Sci.*, 11 (2018) 860-871.
- [13] M. Tang, V. Sarou-Kanian, P. Melin, J.B. Leriche, M. Menetrier, J.M. Tarascon, M. Deschamps, E. Salager, Following lithiation fronts in paramagnetic electrodes with in situ magnetic resonance spectroscopic imaging, *Nat. Commun.*, 7 (2016) 13284.
- [14] Q. Gu, J.A. Kimpton, H.E.A. Brand, Z. Wang, S. Chou, Solving Key Challenges in Battery Research Using In Situ Synchrotron and Neutron Techniques, *Adv. Energy Mater.*, 7 (2017) 1602831.
- [15] D. Liu, Z. Shadike, R. Lin, K. Qian, H. Li, K. Li, S. Wang, Q. Yu, M. Liu, S. Ganapathy, X. Qin, Q.H. Yang, M.

Wagemaker, F. Kang, X.Q. Yang, B. Li, Review of Recent Development of In Situ/Operando Characterization Techniques for Lithium Battery Research, *Adv. Mater.*, 31 (2019) e1806620.

[16] G. Assat, A. Iadecola, C. Delacourt, R. Dedryvère, J.-M. Tarascon, Decoupling Cationic–Anionic Redox Processes in a Model Li-Rich Cathode via Operando X-ray Absorption Spectroscopy, *Chem. Mater.*, 29 (2017) 9714-9724.

[17] S. Kaboli, H. Demers, A. Paoletta, A. Darwiche, M. Dontigny, D. Clement, A. Guerfi, M.L. Trudeau, J.B. Goodenough, K. Zaghbi, Behavior of Solid Electrolyte in Li-Polymer Battery with NMC Cathode via in-Situ Scanning Electron Microscopy, *Nano Lett.*, 20 (2020) 1607-1613.

[18] W. Gao, O. Sel, H. Perrot, Electrochemical and viscoelastic evolution of dodecyl sulfate-doped polypyrrole films during electrochemical cycling, *Electrochim. Acta*, 233 (2017) 262-273.

[19] A. Ispas, R. Peipmann, A. Bund, I. Efimov, On the p-doping of PEDOT layers in various ionic liquids studied by EQCM and acoustic impedance, *Electrochim. Acta*, 54 (2009) 4668-4675.

[20] A.R. Hillman, The EQCM: electrogravimetry with a light touch, *J. Solid State Electrochem.*, 15 (2011) 1647-1660.

[21] T. Liu, L. Lin, X. Bi, L. Tian, K. Yang, J. Liu, M. Li, Z. Chen, J. Lu, K. Amine, K. Xu, F. Pan, In situ quantification of interphasial chemistry in Li-ion battery, *Nat. Nanotechnol.*, 14 (2019) 50-56.

[22] H. Shao, K. Xu, Y.-C. Wu, A. Iadecola, L. Liu, H. Ma, L. Qu, E. Raymundo-Piñero, J. Zhu, Z. Lin, P.-L. Taberna, P. Simon, Unraveling the Charge Storage Mechanism of  $Ti_3C_2T_x$  MXene Electrode in Acidic Electrolyte, *ACS Energy Lett.*, 5 (2020) 2873-2880.

[23] Y.C. Wu, J. Ye, G. Jiang, K. Ni, N. Shu, P.L. Taberna, Y. Zhu, P. Simon, Electrochemical Characterization of Single Layer Graphene/Electrolyte Interface: Effect of Solvent on the Interfacial Capacitance, *Angew. Chem.*, 133 (2021) 2-8.

[24] A. Platek-Mielczarek, E. Frackowiak, K. Fic, Specific carbon/iodide interactions in electrochemical capacitors monitored by EQCM technique, *Energy Environ. Sci.*, 14 (2021) 2381-2393

[25] S. Bourkane, C. Gabrielli, M. Keddad, Kinetic study of electrode processes by ac quartz electrogravimetry, *J. Electroanal. Chem.*, 256 (1988) 471-475.

[26] V. Dargel, N. Shpigel, S. Sigalov, P. Nayak, M.D. Levi, L. Daikhin, D. Aurbach, In situ real-time gravimetric and viscoelastic probing of surface films formation on lithium batteries electrodes, *Nat. Commun.*, 8 (2017) 1389.

[27] N. Shpigel, M.D. Levi, D. Aurbach, EQCM-D technique for complex mechanical characterization of energy storage electrodes: Background and practical guide, *Energy Storage Mater.*, 21 (2019) 399-413.

[28] S. Wang, F. Li, A.D. Easley, J.L. Lutkenhaus, Real-time insight into the doping mechanism of redox-active organic radical polymers, *Nat. Mater.*, 18 (2019) 69-75.

[29] Q. Zhang, M.D. Levi, Q. Dou, Y. Lu, Y. Chai, S. Lei, H. Ji, B. Liu, X. Bu, P. Ma, X. Yan, The charge storage mechanisms of 2D cation-intercalated manganese oxide in different electrolytes, *Adv. Energy Mater.*, 9 (2019) 1802707.

[30] P.G. Kitz, P. Novak, E.J. Berg, Influence of Water Contamination on the SEI Formation in Li-Ion Cells: An Operando EQCM-D Study, *ACS Appl. Mater. Interfaces*, 12 (2020) 15934-15942.

[31] W. Gao, C. Debiemme-Chouvy, M. Lahcini, H. Perrot, O. Sel, Tuning Charge Storage Properties of Supercapacitive Electrodes Evidenced by In Situ Gravimetric and Viscoelastic Explorations, *Anal. Chem.*, 91 (2019) 2885-2893.

[32] K. Solin, M. Borghei, O. Sel, H. Orelma, L.S. Johansson, H. Perrot, O.J. Rojas, Electrically Conductive Thin Films Based on Nanofibrillated Cellulose: Interactions with Water and Applications in Humidity Sensing, *ACS Appl. Mater. Interfaces*, 12 (2020) 36437-36448.

[33] Y. Lyu, X. Wu, K. Wang, Z. Feng, T. Cheng, Y. Liu, M. Wang, R. Chen, L. Xu, J. Zhou, Y. Lu, B. Guo, An Overview on the Advances of  $LiCoO_2$  Cathodes for Lithium - Ion Batteries, *Adv. Energy Mater.*, 11 (2021) 2000982.

[34] W. Gao, N. Krins, C. Laberty-Robert, H. Perrot, O. Sel, Scrutiny of the  $LiCoO_2$  Composite Electrode/Electrolyte Interface by Advanced Electrogravimetry and Implications for Aqueous Li-Ion Batteries, *J. Phys. Chem. C*, 125 (2021) 3859-3867.

- [35] S. Rano, C. Laberty-Robert, K. Ngo, C.M. Sanchez-Sanchez, V. Vivier, Characterization of LiCoO<sub>2</sub> nanoparticle suspensions by single collision events, *Phys. Chem. Chem. Phys.*, 21 (2019) 5416-5423.
- [36] G. Sauerbrey, Verwendung von Schwingquarzen zur Wägung dünner Schichten und zur Mikrowägung, *Zeitschrift für Physik* 155 (1959) 206-222.
- [37] K. Bizet, C. Gabrielli, H. Perrot, Immunodetection by quartz crystal microbalance, *Appl. Biochem. Biotechnol.*, 89 (2000) 139-149.
- [38] H. Muramatsu, A. Egawa, T. Ataka, Reliability of correlation between mass change and resonant frequency change for a viscoelastic-film-coated quartz crystal, *J. Electroanal. Chem.*, 388 (1995) 89-92.
- [39] D. Johannsmann, *The Quartz Crystal Microbalance in Soft Matter Research*, Springer, (2015).
- [40] C. Gabrielli, J.J. García-Jareño, M. Keddad, H. Perrot, F. Vicente, Ac-Electrogravimetry Study of Electroactive Thin Films. I. Application to Prussian Blue, *J. Phys. Chem. B* 106 (2002) 3182-3191.
- [41] C. Gabrielli, J.J. Garcia-Jareno, M. Keddad, H. Perrot, F. Vicente, Ac-electrogravimetry study of electroactive thin films. II. Application to polypyrrole, *J. Phys. Chem. B*, 106 (2002) 3192-3201.
- [42] C.R. Arias, C. Debiemme-Chouvy, C. Gabrielli, C. Laberty-Robert, A. Paillet, H. Perrot, O. Sel, New insights into pseudocapacitive charge-storage mechanisms in Li-Birnessite type MnO<sub>2</sub> monitored by fast quartz crystal microbalance methods, *J. Phys. Chem. C*, 118 (2014) 26551-26559.
- [43] E.M. Halim, R. Demir-Cakan, H. Perrot, M. El Rhazi, O. Sel, Correlation between the interfacial ion dynamics and charge storage properties of poly(ortho-phenylenediamine) electrodes exhibiting high cycling stability, *J. Power Sources*, 438 (2019) 227032.
- [44] E. Duquesne, S. Betelu, C. Bazin, A. Seron, I. Ignatiadis, H. Perrot, O. Sel, C. Debiemme-Chouvy, Insights into Redox Reactions and Ionic Transfers in Nickel/Iron Layered Double Hydroxide in Potassium Hydroxide, *J. Phys. Chem. C*, 124 (2020) 3037-3049.
- [45] P. Lemaire, O. Sel, D. Alves Dalla Corte, A. Iadecola, H. Perrot, J.M. Tarascon, Elucidating the Origin of the Electrochemical Capacity in a Proton-Based Battery HxIrO<sub>4</sub> via Advanced Electrogravimetry, *ACS Appl. Mater. Interfaces*, 12 (2020) 4510-4519.
- [46] V.E. Granstaff, S.J. Martin, Characterization of a thickness-shear mode quartz resonator with multiple nonpiezoelectric layers, *J. Appl. Phys.*, 75 (1994) 1319-1329.
- [47] J.J. García-Jareño, C. Gabrielli, H. Perrot, Validation of the mass response of a quartz crystal microbalance coated with Prussian Blue film for ac electrogravimetry, *Electrochem. Commun.*, 2 (2000) 195-200.
- [48] A.R. Hillman, A. Jackson, S.J. Martin, The problem of uniqueness of fit for viscoelastic films on thickness-shear mode resonator surfaces, *Anal. Chem.*, 73 (2001) 540-549.
- [49] V. Lyutov, V. Gruiia, I. Efimov, A. Bund, V. Tsakova, An acoustic impedance study of PEDOT layers obtained in aqueous solution, *Electrochim. Acta*, 190 (2016) 285-293.
- [50] H.L. Bandey, A.R. Hillman, M.J. Brown, S.J. Martin, Viscoelastic characterization of electroactive polymer films at the electrode/solution interface, *Faraday Discuss.*, 107 (1997) 105-121.
- [51] J.H. Scofield, Hartree-Slater Subshell Photoionization Cross-Sections at 1254 and 1487 EV, *J. Electron Spectrosc. Relat. Phenom.*, 8 (1976) 129-137.
- [52] R.G. Compton, C.E. Banks, *Understanding Voltammetry*, 3rd edn (World Scientific, 2018), *Understanding Voltammetry*, 3rd edn (World Scientific), (2018).
- [53] V. Dargel, N. Jackel, N. Shpigel, S. Sigalov, M.D. Levi, L. Daikhin, V. Presser, D. Aurbach, In situ multilength-scale tracking of dimensional and viscoelastic changes in composite battery electrodes, *ACS Appl. Mater. Interfaces*, 9 (2017) 27664-27675.
- [54] N. Shpigel, S. Sigalov, M. D. Levi, T. Mathis, L. Daikhin, A. Janes, E. Lust, Y. Gogotsi, D. Aurbach, In situ acoustic diagnostics of particle-binder interactions in battery electrodes, *Joule*, 2 (2018) 988-1003.

- [55] A.R. Hillman, M.A. Mohamoud, I. Efimov, Time-temperature superposition and the controlling role of solvation in the viscoelastic properties of polyaniline thin films, *Anal. Chem.*, 83 (2011) 5696-5707.
- [56] L. Dahéron, H. Martinez, R. Dedryvère, I. Baraille, M. Ménétrier, C. Denage, C. Delmas, D. Gonbeau, Surface Properties of  $\text{LiCoO}_2$  Investigated by XPS Analyses and Theoretical Calculations, *J. Phys. Chem. C*, 113 (2009) 5843–5852.
- [57] P. Novák, Electrochemical Insertion of Magnesium in Metal Oxides and Sulfides from Aprotic Electrolytes, *J. Electrochem. Soc.*, 140 (1993) 140-144.
- [58] Y. Mizuno, M. Okubo, E. Hosono, T. Kudo, H. Zhou, K. Oh-ishi, Suppressed Activation Energy for Interfacial Charge Transfer of a Prussian Blue Analog Thin Film Electrode with Hydrated Ions ( $\text{Li}^+$ ,  $\text{Na}^+$ , and  $\text{Mg}^{2+}$ ), *J. Phys. Chem. C*, 117 (2013) 10877-10882.
- [59] J. Song, M. Noked, E. Gillette, J. Duay, G. Rubloff, S.B. Lee, Activation of a  $\text{MnO}_2$  cathode by water-stimulated  $\text{Mg}^{2+}$  insertion for a magnesium ion battery, *Phys. Chem. Chem. Phys.*, 17 (2015) 5256-5264.

Journal Pre-proof

## Graphical Abstract

